# Unified spectrum of tropical rainfall and waves in a simple stochastic model

**Samuel N. Stechmann[1,2] and Scott Hottovy[3]**

**Submitted on April 21, 2017**
**Revised on August 18, 2017**
**Revised on September 19, 2017**

[1]Department of Mathematics, University of Wisconsin–Madison, Madison, Wisconsin, USA.
[2]Department of Atmospheric and Oceanic Sciences, University of Wisconsin–Madison, Madison, Wisconsin, USA.
[3]Department of Mathematics, United States Naval Academy, Annapolis, Maryland, USA

**Key Points:**

- Linear stochastic model reproduces tropical dynamics, unified from synoptic to planetary scales
- Differing roles of lower- and mid-tropospheric water vapor are key physical processes
- Antiresonance is shown to inhibit rainfall oscillations at dry wave frequencies

Corresponding author: Samuel N. Stechmann, `stechmann@wisc.edu`

## Abstract

In the tropics, rainfall is coupled with atmospheric dynamics in ways that are not fully understood, and often different mechanisms are proposed to underlie different modes of variability. Here, it is shown that a unified model with a simple form can produce many different modes of variability. In particular, this includes the Madden–Julian oscillation and convectively coupled equatorial waves. The model predicts the length scales, time scales, structures, and spatiotemporal variability of these modes reasonably well for a simple model. Furthermore, the model produces a background spectrum of rainfall that resembles spatiotemporal red noise and is only weakly coupled with wave dynamics. The full spectrum is also shown to be shaped by antiresonance, whereby rainfall oscillations are prevented from occurring at the oscillation frequencies of dry waves. To produce all of these aspects simultaneously, a key factor is differing roles of lower and middle tropospheric water vapor.


## 1 Introduction

Tropical rainfall is often organized into clusters, and the clusters have sizes and lifetimes that are seemingly random [*Mapes and Houze*, 1993; *Peters et al.*, 2009]. Indeed, upon initial inspection, tropical rainfall appears to have statistics that resemble spatiotemporal red noise [*Takayabu*, 1994; *Wheeler and Kiladis*, 1999; *Hottovy and Stechmann*, 2015].

A more detailed inspection reveals that tropical rainfall is also coupled to atmospheric waves [*Takayabu*, 1994; *Wheeler and Kiladis*, 1999]. The waves can have a variety of length scales and time scales, and two common examples are convectively coupled equatorial waves (CCEWs), which occur on synoptic scales of days and thousands of kilometers [*Kiladis et al.*, 2009], and the Madden–Julian Oscillation (MJO), which occurs on planetary and intraseasonal scales of months and tens of thousands of kilometers [*Madden and Julian*, 1971, 1972; *Zhang*, 2005].

The MJO and CCEWs are intimately connected with many of the most important weather and climate phenomena. For example, CCEWs influence the formation of tropical cyclones [*Dickinson and Molinari*, 2002; *Bessafi and Wheeler*, 2006; *Frank and Roundy*, 2006]. The MJO also impacts tropical cyclones [*Liebmann et al.*, 1994; *Maloney and Hartmann*, 2000], El Niño–Southern Oscillation [*Hendon et al.*, 2007], active and break phases of monsoons [*Lau and Waliser*, 2012], midlatitude weather and its predictability [*Jones*, 2000; *Jones et al.*, 2004], and ocean biogeochemistry [*Waliser et al.*, 2005].

To what extent are CCEWs and the MJO understood theoretically and simulated faithfully in global climate models (GCMs) and simplified models? Many GCM simulations continue to show deficiencies in their representation of CCEWs and the MJO [*Slingo et al.*, 1996; *Lin et al.*, 2006; *Straub et al.*, 2010; *Hung et al.*, 2013], although some recent improvements and success have also been seen [*Grabowski*, 2001; *Khairoutdinov et al.*, 2005; *Benedict and Randall*, 2009; *Khouider et al.*, 2011; *Hung et al.*, 2013; *Deng et al.*, 2015]. Simplified models have been proposed and typically describe either CCEWs or the MJO. For example, CCEW models include convective adjustment and quasi-equilibrium theory [*Gill*, 1982; *Emanuel et al.*, 1994; *Neelin and Zeng*, 2000] and more complex models that include multiple cloud types such as stratiform [*Mapes*, 2000] and also congestus [*Khouider and Majda*, 2006a, 2007, 2008]. On the other hand, MJO models include boundary-layer frictional convergence [*Wang and Rui*, 1990; *Salby et al.*, 1994], moisture mode theories [*Raymond and Fuchs*, 2009; *Sobel and Maloney*, 2013; *Adames and Kim*, 2016], and the skeleton model [*Majda and Stechmann*, 2009a, 2011].

The present paper describes a unified model for CCEWs and the MJO together. The main physical process is simply convective adjustment, although here it is used, importantly, in a framework with two vertical levels of moisture. It will be shown that this model produces both an MJO and CCEWs with length scales, time scales, structures, and spatiotemporal variability that are reasonably realistic for a simple model.

## 2 Model description

The model equations are

$$
\begin{aligned}
\frac{\partial \mathbf{u}}{\partial t} + y\mathbf{u}^{\perp} - \nabla\theta &= -\frac{1}{\tau_u}\mathbf{u} && (1)\\
\frac{\partial \theta}{\partial t} - \nabla\cdot\mathbf{u} &= \frac{1}{\tau_{low}}q_{low} + \frac{1}{\tau_{mid}}q_{mid} - \frac{1}{\tau_\theta}\theta && (2)\\
\frac{\partial q_{low}}{\partial t} + \tilde{Q}_{low}\nabla\cdot\mathbf{u} &= -\frac{1}{\tau_{low}}q_{low} + b_{low}\nabla^2 q_{low} + F_{low} + D_{low}\dot{W}_{low} && (3)\\
\frac{\partial q_{mid}}{\partial t} + \tilde{Q}_{mid}\nabla\cdot\mathbf{u} &= -\frac{1}{\tau_{mid}}q_{mid} + b_{mid}\nabla^2 q_{mid} + F_{mid} + D_{mid}\dot{W}_{mid} && (4)
\end{aligned}
$$

where $\mathbf{u} = (u, v)^T$ is the vector of zonal and meridional velocity components, respectively, of the first vertical baroclinic mode, $\theta$ is the first baroclinic potential temperature, and $q_{low}$ and $q_{mid}$ are the mixing ratios of water in the lower and middle troposphere, respectively. The Coriolis term is written, under the equatorial beta-plane approximation, as $y\mathbf{u}^{\perp}$, where $\mathbf{u}^{\perp} = (-v, u)^T$. The equations have been nondimensionalized using standard equatorial reference scales following *Stechmann et al.* [2008], *Majda and Stechmann* [2009a], and *Stechmann and Majda* [2015]. The moisture forcing includes deterministic components, $F_{low}(x, y)$ and $F_{mid}(x, y)$, which are taken to be time-independent here for simplicity, and stochastic components proportional to $\dot{W}_{low}(x, y, t)$ and $\dot{W}_{mid}(x, y, t)$. The stochastic components are chosen to be independent of each other for simplicity, and each is a spatiotemporal white noise; i.e., each of $\dot{W}_{low}$ and $\dot{W}_{mid}$ has a mean of 0 and a covariance of $\delta(x-x')\delta(y-y')\delta(t-t')$. The stochastic moisture forcing is, in part, representative of mesoscale convective processes that are not represented by the larger-scale dynamics in (1)–(4); relative to the larger-scale dynamics in (1)–(4), it is reasonable to assume that such processes are approximately spatiotemporally uncorrelated.

The dynamical core of (1)–(4) can be derived from the three-dimensional primitive equations, using a modification of the methods of *Stechmann et al.* [2008], with the addition that water vapor $q(x, y, z, t)$ is also included and expanded in vertical baroclinic modes; see Supporting Information (SI). In the derivation, the vertical-level variables, $q_{low}$ and $q_{mid}$, are related to first- and second-baroclinic-mode variables via a discrete sine transform. Such an approach differs from derivations that have used a single vertically-averaged moisture variable [*Neelin and Zeng*, 2000; *Khouider and Majda*, 2006a,b]; other models have also incorporated multiple vertical moisture levels [e.g., *Khouider and Moncrieff*, 2015; *Thual and Majda*, 2015]. The physical meaning of $\tilde{Q}_{low}$ and $\tilde{Q}_{mid}$ is essentially the vertical derivative of the background profile $q_{bg}(z)$ of water vapor mixing ratio; see the SI for details.

In relation to some earlier models, one can view the model in (1)–(4) as a coupling of (I) a traditional model of convective adjustment for $\mathbf{u}, \theta$, and $q_{low}$ [e.g., *Betts and Miller*, 1986; *Neelin and Yu*, 1994] and (II) a recently proposed model of the background spectrum of tropical convection for $q_{mid}$ [*Hottovy and Stechmann*, 2015]. Component I influences component II via the moisture convergence term $\tilde{Q}_{mid}\nabla\cdot\mathbf{u}$ in (4), and vice versa via the cloud latent heating term $\tau_{mid}^{-1}q_{mid}$ in (2). However, despite this appearance as a combination of earlier models, the dynamical core in its entirety can be derived systematically through an expansion in vertical baroclinic modes, as described in the previous paragraph and the SI. Also, as a whole, the model in (1)–(4) is new, to the best of our knowledge. Further comparisons with other models are described in the SI.

The parameters in the present model in (1)–(4) are chosen in the following way. The parameters in component I take on standard values: $\tilde{Q}_{low} = 0.9$, as in *Neelin and Yu* [1994], *Khouider and Majda* [2006a], and *Majda and Stechmann* [2009a], and $\tau_{low} = 4$ hours, similar to the values used by *Neelin and Yu* [1994] and *Khouider and Majda* [2006a]. The parameters in component II take on values similar to *Hottovy and Stechmann* [2015] and are calibrated by comparison with the climatological variance, i.e., the power spectrum of tropical rainfall [*Takayabu*, 1994; *Wheeler and Kiladis*, 1999; *Lin et al.*, 2006]: $\tau_{mid} = 1.33$ days and $b_{mid} =$

60.6 km$^2$ s$^{-1}$ (0.8 in nondimensional units). The parameters $\tau_u = \tau_\theta = 16$ days were calibrated similarly and are consistent with the results of *Stechmann and Ogrosky* [2014]. In addition, the new term $\tilde{Q}_{mid}\nabla\cdot\mathbf{u}$ in (4) introduces a new parameter, $\tilde{Q}_{mid} = 0.45$; this value is smaller than $\tilde{Q}_{low} = 0.9$ and reflects two differences in mid-tropospheric moisture compared to lower tropospheric moisture: (i) a weaker vertical gradient, and (ii) a weaker coupling with first-baroclinic horizontal convergence. Finally, the new terms $b_{low}\nabla^2 q_{low}$ and $D_{low}\dot{W}_{low}$ in (3) were added as a simple parameterization of turbulent advection–diffusion [*Majda and Kramer*, 1999; *DelSole*, 2004; *Majda and Grote*, 2007, 2009], similar to the terms $b_{mid}\nabla^2 q_{mid}$ and $D_{mid}\dot{W}_{mid}$ in (4) [*Hottovy and Stechmann*, 2015] and calibrated in the same way to give values of $b_{low} = 7.58$ km$^2$ s$^{-1}$ (0.1 in nondimensional units) and, for simplicity, $D_{low} = D_{mid} = 0.0663$ g kg$^{-1}$ h$^{-1/2}$ (0.03 in nondimensional units). The values of $F_{low}(x, y)$ and $F_{mid}(x, y)$ are chosen as idealized versions of moisture sources (see SI) [*Ogrosky and Stechmann*, 2015a; *Stachnik et al.*, 2015], and they create a Walker circulation that aids the comparison between model output and observational data (although note that $F_{low}(x, y)$ and $F_{mid}(x, y)$ affect the steady mean state, i.e. the Walker circulation, but they do not affect the unsteady dynamics and variances of the model variables). Finally, note that this set of standard parameters leads to eigenmodes that are all damped, which allows the model to be analyzed in a statistically stationary state.

Solutions to the stochastic model in (1)–(4) can be obtained semi-analytically. In brief, the equations are expanded in terms of the leading meridional basis functions of traditional equatorial wave theory, following *Matsuno* [1966], *Majda* [2003], and *Ogrosky and Stechmann* [2015b], and the water vapor equations are similarly expanded, following *Khouider and Majda* [2008], *Majda and Stechmann* [2009a], and *Stechmann and Majda* [2015]. The result is a system of stochastic partial differential equations (SPDEs) as functions of $x$ and $t$, which are linear with constant coefficients and can be solved using Fourier transforms [*Majda and Grote*, 2007, 2009; *Hottovy and Stechmann*, 2015]. Further details of the methodology are described in the SI [*Gill*, 1980; *Chao*, 1987; *Yu and Neelin*, 1994; *Haertel and Kiladis*, 2004; *Majda and Biello*, 2004; *Biello and Majda*, 2005; *Majda et al.*, 2007; *Holloway and Neelin*, 2009; *Ajayamohan et al.*, 2013; *Stechmann et al.*, 2013; *Thual et al.*, 2014; *Jiang et al.*, 2016].

## 3 Stochastic variability and composite structures

Examples of the model solutions are shown in Fig. 1, and they display many features in common with observed dynamics; e.g., see Fig. 1 of *Nakazawa* [1986] and Fig. 5 of *Roundy and Frank* [2004]. The figure here has been formatted for direct comparison with Fig. 2 of *Zhang* [2005]. At the crudest level, the dynamics appear to be incoherent and random. At a more detailed level, many coherent wave signals can be identified and are comparable to the MJO and CCEW signals seen in observational data in terms of length scales, propagation speeds, and to some extent even duration or lifetime of wave events.

Composite structures of two prominent wave types—the MJO and convectively coupled Kelvin wave (CCKW)—are shown in Fig. 2, and they display many of the main features seen in composites created from observational data. For computing the composites, the methods are essentially the same as standard lagged regression techniques, except here the lagged regression coefficients can be determined semi-analytically as a stationary spatiotemporal covariance, whereas they must be estimated statistically when analyzing observational data [e.g., *Wheeler et al.*, 2000].

First, Fig. 2a shows the composite structure of the model MJO, which is comparable to composites constructed from observational data [e.g., *Hendon and Salby*, 1994]. In particular, four off-equatorial gyres surround an equatorial precipitation anomaly and resemble a Rossby wave's circulation pattern (although the MJO propagates eastward whereas Rossby waves propagate westward). Furthermore, the model composite also contains aspects of a Kelvin wave structure near the equator, such as the positive geopotential anomaly on the equator, which lies in between negative Rossby-like geopotential height anomalies off the equator.

Second, Fig. 2b shows the composite structure of the model CCKW, which is comparable to CCKW composites constructed from observational data [*Takayabu and Murakami*, 1991; *Wheeler et al.*, 2000; *Straub and Kiladis*, 2002; *Kiladis et al.*, 2009]. The main features include zonal wind anomalies confined near the equator and a precipitation maximum located near the maximum of convergence. The vertical structure here has a first-baroclinic-mode form, as the model is formulated with such a vertical structure, so it is expected that the vertical tilts of observed CCKWs are not represented here (although a vertical tilt will be seen in a later figure in the water vapor of the CCKW eigenvector). Also, while the phase relationships and shapes of the fields (winds, geopotential height, etc.) compare reasonably well with observational composites, some relative amplitudes of the fields have some differences from what is seen in observational composites, at least in part because such a detailed comparison is challenging due to the simplified vertical structure of the model.

The propagation of the model MJO and CCKW are shown in composite form in Fig. 2e,f. Their propagation speeds are approximately 4 and 15 m/s, respectively, similar to the speeds seen in observational composites of MJO propagation [*Hendon and Salby*, 1994; *Zhang*, 2005; *Lin et al.*, 2006; *Hung et al.*, 2013] and CCKW propagation [*Wheeler et al.*, 2000; *Straub and Kiladis*, 2002, 2003; *Straub et al.*, 2010].

The variance – i.e., the spectral power – of precipitation is shown in Fig. 3 for each zonal wavenumber $k$ and temporal frequency $\omega$. The raw power spectrum in Fig. 3a has many features in common with observed power spectra [*Takayabu*, 1994; *Wheeler and Kiladis*, 1999], and the figure axes have been formatted for direct comparison with Figs. 5a,b of *Lin et al.* [2006]. At the crudest level, it resembles the spectrum of spatiotemporal "red noise," since the power is greatest for lower frequencies (or "redder" frequencies in analogy with visible light waves) [*Hottovy and Stechmann*, 2015]. At a more detailed level, the power appears to be enhanced at certain frequencies; to isolate these enhancements, we follow the method of *Wheeler and Kiladis* [1999] to remove the "background" or "red-noise" contribution of the spectrum (Fig. 3b), which leads to the anomalous spectral power shown in Fig. 3c. The figure axes here have been formatted for direct comparison with Figs. 6a,b of *Lin et al.* [2006]. This model result resembles the observed result [*Wheeler and Kiladis*, 1999; *Kiladis et al.*, 2009] in many ways. In particular, spectral peaks are seen at roughly the wavenumbers and frequencies of the MJO and CCEWs.

## 4 MJO and CCEW eigenmodes

The MJO and CCEWs in Figs. 1–3 arise from the eigenmodes of the deterministic, unforced part of the model in (1)–(4). Two of the eigenmodes resemble the MJO and CCKW, and their structures are shown in Fig. 4a,b. (Another type of CCKW eigenmode is shown in the SI in Fig. S1.) These structures are very similar to the statistical composites shown earlier in Fig. 2 and Sec. 3, which suggests these eigenmodes are the dominant contributors to the statistical composite structures.

The dispersion curves and decay time scales of the eigenmodes are shown in Fig. 4e. At a broad level, a mean feature is that the dispersion curves are often in alignment with the peaks in spectral power. This alignment is related to resonance, as described in section 6 below.

## 5 Changes in wave properties under different background moisture states

The MJO and CCKW properties can change under different background moisture profiles. Before describing these aspects of the model, we briefly describe some related behavior seen in observational data analyses.

Beyond the viewpoint of the MJO and CCKW as distinct modes, some analyses of observational data also suggest a continuum of modes between the MJO and CCKWs, or transitions between these modes, or modes that are hybrid MJO–CCKWs [*Roundy*, 2012a,b, 2014; *Sobel and Kim*, 2012]. Furthermore, different background states are related to differences in the occurrence of the MJO, CCKWs, or hybrid MJO–CCKWs. *Roundy* [2014] shows that MJO events are associated with a more moist mid-troposphere, and hybrid MJO–CCKW events are associated with a relatively less moist mid-troposphere.

A similar association is also seen in the model: the MJO is associated with larger values of $\tilde{Q}_{mid}$, and a hybrid MJO–CCKW is associated with smaller values of $\tilde{Q}_{mid}$. A case of a hybrid MJO–CCKW is illustrated in the SI in Fig. S2, for the lower value of $\tilde{Q}_{mid} = 0.1$, in comparison to the standard value of $\tilde{Q}_{mid} = 0.45$.

Instability of the MJO can result, on the other hand, if the mid-troposphere is more moist. More specifically, if $\tilde{Q}_{mid}$ takes the larger values of 0.5, 0.6, or 0.7, then 1, 2, or 3 zonal wavenumbers of the MJO become unstable, respectively.

It is interesting that these changes in the MJO and CCEWs result from only changes to the background water vapor profile. It is not necessary here to invoke any more complex physical mechanisms such as cloud–radiation feedback, wind-induced surface heat exchange, boundary-layer frictional convergence, etc. One can interpret different values of $\tilde{Q}_{mid}$ as representing changes in the atmospheric base state in different regions of the tropics or in different seasons.

## 6 Resonance and anti-resonance in shaping the power spectrum

The power spectrum of tropical convection has peaks, relative to a background power spectrum, and the peaks are roughly aligned with theoretical wave dispersion curves. This alignment has been noted in observational data analyses [*Takayabu*, 1994; *Wheeler and Kiladis*, 1999], in which the dry shallow water equations (SWEs) were used to indicate theoretical dispersion curves for comparison.

Nevertheless, while the dry SWEs are useful for their simplicity and analytical solutions, they do not account for many details of the observed spectral peaks. For example, the waves of the dry SWEs are all neutrally stable, which is somewhat at odds with the different magnitudes of spectral power seen for different wave types (e.g., Kelvin versus Rossby) and different wavelengths (e.g., planetary versus synoptic versus mesoscales).

Resonance is the source of the spectral peaks in Fig. 3 for the present model. In brief, the spatiotemporal white noise, $\dot{W}_{low}$ and $\dot{W}_{mid}$, provides a forcing of all possible wavelengths and frequencies, and the spectral peaks arise near some of the model's natural frequencies. The resonant peaks have finite amplitude rather than infinite amplitude because the present model's waves are all damped.

The magnitudes of the spectral peaks are influenced primarily by two factors. First, the damping rate is different for each eigenmode (see Fig. 4e), and a weaker damping rate allows a larger resonant response and a larger spectral peak. For example, this effect contributes to the larger spectral peak of the MJO compared to the CCKW. Second, a larger forcing amplitude allows a larger resonant response and a larger spectral peak. The forcing amplitude for each eigenmode is related to the contribution of water vapor to the eigenmode, since the forcing $\dot{W}_{low}$ and $\dot{W}_{mid}$ is present only in the water vapor equations. Therefore, if an eigenmode's structure is relatively "dry," then it can have a weak spectral peak even if it is only weakly damped. "Moist" eigenmodes such as the MJO and CCKWs have the largest spectral peaks.

In addition, *anti-resonance* can create spectral *valleys*. For example, a spectral valley is indicated in Fig. 3a by a white dashed line along $\omega = c_d k$, where $c_d = 50$ m/s is the speed of a dry Kelvin wave. Such a valley can also be seen in observational data analyses, such as Figs. 1b and 3b of *Wheeler and Kiladis* [1999] and Figs. 5a and 6a of *Lin et al.* [2006]. While spectral valleys have received much less attention than spectral peaks, the shape of the power spectrum is influenced by both peaks and valleys.

The anti-resonance mechanism involves a coupled system. In the present context, it is a coupling between the dry variables $(\mathbf{u}, \theta)$ and water vapor $(q)$. An idealization of the coupled system can be written as the ordinary differential equations

$$\frac{d^2u}{dt^2} + \omega_d^2 u = q \tag{5}$$

$$\frac{d^2q}{dt^2} + au = F_0 \cos \omega_f t. \tag{6}$$

Antiresonance arises when the forcing frequency $\omega_f$ is equal to the dry dynamical core's oscillation frequency $\omega_d$. In this case, in the forced wave response, both $u$ and $q$ are proportional to $\cos \omega_f t$, but one can see from (5) that the amplitude of $q$ is zero. In the real atmosphere and the stochastic model (1)–(4), the amplitude of $q$ would not be exactly zero, since damping, nonlinearity, and other mechanisms introduce discrepancies from the idealized anti-resonance scenario; but anti-resonance can still create spectral valleys. In short, since rainfall acts as a heat source for the dry dynamical core, rainfall oscillations are suppressed at the natural frequencies of the dry dynamical core.

Several features of tropical convection can possibly be influenced by anti-resonance. As one example, in analyses of CCEWs [e.g., *Tulich and Kiladis*, 2012], westward inertio-gravity waves are seen to have significantly greater spectral power than eastward inertio-gravity (EIG) waves. One possible explanation for this is that CCEWs can be influenced by vertical shear of zonal wind [*Majda and Stechmann*, 2009b; *Stechmann and Majda*, 2009; *Han and Khouider*, 2010; *Tulich and Kiladis*, 2012; *Dias and Kiladis*, 2014]. Anti-resonance may also have an influence, since it suppresses rainfall oscillations near the frequencies of dry Kelvin waves, which overlap with the frequencies of convectively coupled EIG waves. As a second example, recall that the MJO has a strong spectral peak at eastward wavenumbers $1 \leq k \leq 3$, and convectively coupled equatorial Rossby waves have a spectral peak at westward wavenumbers $-4 \leq k \leq -3$; e.g., see Fig. 3 of the present paper or Fig. 3b of *Wheeler and Kiladis* [1999]. It is possible that the dearth of spectral power at westward wavenumbers $k = -1$ and $-2$ is influenced by anti-resonance from dry equatorial Rossby waves.

## 7 Discussion and Conclusions

In summary, a simple model was presented and shown to simulate the basic features of both the MJO and CCEWs, including their length scales, time scales, structures, and spatiotemporal variability. This suggests the MJO and CCEWs could arise from simple physical processes such as convective adjustment.

A key element of the model is the differing roles of lower- and mid-tropospheric moisture. The results have potential implications for global climate models, whose representations of the MJO and CCEWs are being analyzed for links with vertical structure and associated processes [*Klingaman et al.*, 2015].

Also, by analyzing the shape of the power spectrum, key roles were identified here for both resonance and anti-resonance. Anti-resonance was shown to suppress rainfall oscillations at dry wave frequencies, which can create spectral valleys.

These aspects were found in a model that is linear and that uses a simple vertical structure. As a result, some details of the MJO and CCEWs are not represented, such as absolute rainfall that is strictly positive, and vertical tilts in the structures of winds and temperature (although vertically tilted water vapor was sometimes seen). To add further realistic details, it would be interesting in the future to include additional physical processes into the model (see SI for comparisons to other models), such as a nonlinear threshold in the convective parameterization and refined vertical structures.

In addition to the synoptic and planetary scales analyzed here, mesoscale cloud features would be expected to arise from the model if a smaller grid spacing were utilized. In particular, in a similar model that ignored wave dynamics, *Hottovy and Stechmann* [2015] showed that the model reproduces many statistics of mesoscale cloud clusters and rainfall, such as a power-law distribution of cloud cluster areas [*Peters et al.*, 2009; *Wood and Field*, 2011]. Taken together, these results suggest that the present model has a unified representation of many tropical convection statistics across three or four orders of magnitude of scales, from planetary to synoptic to mesoscales.

## Acknowledgments

The research of S.N.S. is partially supported by a Sloan Research Fellowship, ONR Young Investigator Award N00014-12-1-0744, and ONR MURI grant N00014-12-1-0912. S.H. was supported as a postdoctoral researcher by the ONR grants. Computing resources were partially supported by ONR DURIP grant N00014-14-1-0251 and the University of Wisconsin-Madison Advanced Computing Initiative. The authors thank A. Majda for comments on an early draft of the manuscript, as well as two anonymous reviewers. The data used are listed in the figures, supplements, and references.

## References

Adames, Á. F., and D. Kim (2016), The MJO as a dispersive, convectively coupled moisture wave: Theory and observations, *J. Atmos. Sci.*, *73*(3), 913–941.

Ajayamohan, R. S., B. Khouider, and A. J. Majda (2013), Realistic initiation and dynamics of the Madden–Julian Oscillation in a coarse resolution aquaplanet GCM, *Geophys. Res. Lett.*, *40*(23), 6252–6257.

Benedict, J., and D. Randall (2009), Structure of the Madden–Julian oscillation in the superparameterized CAM, *J. Atmos. Sci.*, *66*(11), 3277–3296.

Bessafi, M., and M. C. Wheeler (2006), Modulation of south Indian Ocean tropical cyclones by the Madden–Julian oscillation and convectively coupled equatorial waves, *Mon. Wea. Rev.*, *134*(2), 638–656.

Betts, A. K., and M. J. Miller (1986), A new convective adjustment scheme. Part II: Single column tests using GATE wave, BOMEX, ATEX and arctic airmass data sets, *Q. J. Roy. Met. Soc.*, *112*, 693–709.

Biello, J. A., and A. J. Majda (2005), A new multiscale model for the Madden–Julian oscillation., *J. Atmos. Sci.*, *62*, 1694–1721.

Chao, W. C. (1987), On the origin of the tropical intraseasonal oscillation., *J. Atmos. Sci.*, *44*, 1940–1949.

DelSole, T. (2004), Stochastic models of quasigeostrophic turbulence, *Surv. Geophys.*, *25*(2), 107–149, doi:10.1023/B:GEOP.0000028160.75549.0d.

Deng, Q., B. Khouider, and A. J. Majda (2015), The MJO in a coarse-resolution GCM with a stochastic multicloud parameterization, *J. Atmos. Sci.*, *72*, 55–74, doi:10.1175/JAS-D-14-0120.1.

Dias, J., and G. N. Kiladis (2014), Influence of the basic state zonal flow on convectively coupled equatorial waves, *Geophys. Res. Lett.*, *41*(19), 6904–6913, doi:10.1002/2014GL061476.

Dickinson, M., and J. Molinari (2002), Mixed Rossby–gravity waves and western Pacific tropical cyclogenesis. Part I: Synoptic evolution, *J. Atmos. Sci.*, *59*(14), 2183–2196.

Emanuel, K. A., J. D. Neelin, and C. S. Bretherton (1994), On large-scale circulations in convecting atmospheres, *Q. J. Roy. Met. Soc.*, *120*(519), 1111–1143.

Frank, W. M., and P. E. Roundy (2006), The role of tropical waves in tropical cyclogenesis, *Monthly Weather Review*, *134*(9), 2397–2417.

Gill, A. E. (1980), Some simple solutions for heat-induced tropical circulation, *Q. J. Royal Meteor. Soc.*, *106*(449), 447–462.

Gill, A. E. (1982), Studies of moisture effects in simple atmospheric models: The stable case, *Geophys. Astrophys. Fluid Dynam.*, *19*(1-2), 119–152.

Grabowski, W. W. (2001), Coupling cloud processes with the large-scale dynamics using the cloud-resolving convection parameterization (CRCP)., *J. Atmos. Sci.*, *58*, 978–997.

Haertel, P. T., and G. N. Kiladis (2004), Dynamics of 2-day equatorial waves., *J. Atmos. Sci.*, *61*, 2707–2721.

Han, Y., and B. Khouider (2010), Convectively coupled waves in a sheared environment, *J. Atmos. Sci.*, *67*(9), 2913–2942, doi:10.1175/2010JAS3335.1.

Hendon, H. H., and M. L. Salby (1994), The life cycle of the Madden–Julian oscillation., *J. Atmos. Sci.*, *51*, 2225–2237.

Hendon, H. H., M. C. Wheeler, and C. Zhang (2007), Seasonal dependence of the MJO–ENS relationship, *J. Climate*, *20*(3), 531–543.

Holloway, C. E., and J. D. Neelin (2009), Moisture vertical structure, column water vapor, and tropical deep convection, *J. Atmos. Sci.*, *66*(6), 1665–1683.

Hottovy, S. A., and S. N. Stechmann (2015), A spatiotemporal stochastic model for tropical precipitation and water vapor dynamics, *J. Atmos. Sci.*, *72*, 4721–4738, doi:10.1175/JAS-D-15-0119.1.

Hung, M.-P., J.-L. Lin, W. Wang, D. Kim, T. Shinoda, and S. J. Weaver (2013), MJO and convectively coupled equatorial waves simulated by CMIP5 climate models, *J. Climate*, *26*(17), 6185–6214.

Jiang, X., M. Zhao, E. D. Maloney, and D. E. Waliser (2016), Convective moisture adjustment time scale as a key factor in regulating model amplitude of the Madden-Julian oscillation, *Geophys. Res. Lett.*, *43*(19).

Jones, C. (2000), Occurrence of extreme precipitation events in California and relationships with the Madden–Julian oscillation, *J. Climate*, *13*(20), 3576–3587.

Jones, C., D. E. Waliser, K. M. Lau, and W. Stern (2004), The Madden–Julian oscillation and its impact on Northern Hemisphere weather predictability, *Mon. Wea. Rev.*, *132*(6), 1462–1471.

Khairoutdinov, M., D. Randall, and C. Demott (2005), Simulations of the atmospheric general circulation using a cloud-resolving model as a superparameterization of physical processes., *Journal of Atmospheric Sciences*, *62*, 2136–2154.

Khouider, B., and A. J. Majda (2006a), A simple multicloud parameterization for convectively coupled tropical waves. Part I: Linear analysis, *J. Atmos. Sci.*, *63*, 1308–1323.

Khouider, B., and A. J. Majda (2006b), Multicloud convective parameterizations with crude vertical structure, *Theor. Comp. Fluid Dyn.*, *20*, 351–375.

Khouider, B., and A. J. Majda (2007), A simple multicloud parameterization for convectively coupled tropical waves. Part II: Nonlinear simulations, *J. Atmos. Sci.*, *64*, 381–400.

Khouider, B., and A. J. Majda (2008), Equatorial convectively coupled waves in a simple multicloud model, *J. Atmos. Sci.*, *65*, 3376–3397.

Khouider, B., and M. W. Moncrieff (2015), Organized convection parameterization for the ITCZ, *J. Atmos. Sci.*, *72*(8), 3073–3096, doi:10.1175/JAS-D-15-0006.1.

Khouider, B., A. St-Cyr, A. J. Majda, and J. Tribbia (2011), The MJO and convectively coupled waves in a coarse-resolution GCM with a simple multicloud parameterization, *J. Atmos. Sci.*, *68*, 240–264.

Kiladis, G. N., M. C. Wheeler, P. T. Haertel, K. H. Straub, and P. E. Roundy (2009), Convectively coupled equatorial waves, *Rev. Geophys.*, *47*, RG2003, doi:10.1029/2008RG000266.

Klingaman, N. P., X. Jiang, P. K. Xavier, J. Petch, D. Waliser, and S. J. Woolnough (2015), Vertical structure and physical processes of the Madden-Julian oscillation: Synthesis and summary, *J. Geophys. Res. Atmos.*, *120*(10), 4671–4689.

Lau, W. K. M., and D. E. Waliser (Eds.) (2012), *Intraseasonal Variability in the Atmosphere–Ocean Climate System*, 2nd ed., Springer, Berlin.

Liebmann, B., H. H. Hendon, and J. D. Glick (1994), The relationship between tropical cyclones of the western Pacific and Indian Oceans and the Madden–Julian oscillation, *J. Met. Soc. Japan*, *72*(3), 401–412.

Lin, J.-L., G. N. Kiladis, B. E. Mapes, K. M. Weickmann, K. R. Sperber, W. Lin, M. Wheeler, S. D. Schubert, A. Del Genio, L. J. Donner, S. Emori, J.-F. Gueremy, F. Hourdin, P. J. Rasch, E. Roeckner, and J. F. Scinocca (2006), Tropical intraseasonal variability in 14 IPCC AR4 climate models Part I: Convective signals, *J. Climate*, *19*, 2665–2690.

Madden, R. A., and P. R. Julian (1971), Detection of a 40–50 day oscillation in the zonal wind in the tropical Pacific, *J. Atmos. Sci.*, *28*(5), 702–708.

Madden, R. A., and P. R. Julian (1972), Description of global-scale circulation cells in the Tropics with a 40–50 day period., *J. Atmos. Sci.*, *29*, 1109–1123.

Majda, A. J. (2003), *Introduction to PDEs and Waves for the Atmosphere and Ocean*, *Courant Lecture Notes in Mathematics*, vol. 9, x+234 pp., American Mathematical Society, Providence.

Majda, A. J., and J. A. Biello (2004), A multiscale model for the intraseasonal oscillation, *Proc. Natl. Acad. Sci. USA*, *101*(14), 4736–4741.

Majda, A. J., and M. J. Grote (2007), Explicit off-line criteria for stable accurate time filtering of strongly unstable spatially extended systems, *Proc. Natl. Acad. Sci. USA*, *104*, 1124–1129.

Majda, A. J., and M. J. Grote (2009), Mathematical test models for superparametrization in anisotropic turbulence, *Proc. Natl. Acad. Sci. USA*, *106*(14), 5470–5474.

Majda, A. J., and P. R. Kramer (1999), Simplified models for turbulent diffusion: theory, numerical modelling, and physical phenomena, *Phys. Rep.*, *314*(4), 237–574, doi:10.1016/S0370-1573(98)00083-0.

Majda, A. J., and S. N. Stechmann (2009a), The skeleton of tropical intraseasonal oscillations, *Proc. Natl. Acad. Sci. USA*, *106*(21), 8417–8422.

Majda, A. J., and S. N. Stechmann (2009b), A simple dynamical model with features of convective momentum transport, *J. Atmos. Sci.*, *66*, 373–392.

Majda, A. J., and S. N. Stechmann (2011), Nonlinear dynamics and regional variations in the MJO skeleton, *J. Atmos. Sci.*, *68*, 3053–3071.

Majda, A. J., S. N. Stechmann, and B. Khouider (2007), Madden–Julian Oscillation analog and intraseasonal variability in a multicloud model above the equator, *Proc. Natl. Acad. Sci. USA*, *104*(24), 9919–9924.

Maloney, E. D., and D. L. Hartmann (2000), Modulation of hurricane activity in the Gulf of Mexico by the Madden–Julian oscillation, *Science*, *287*(5460), 2002–2004.

Mapes, B. E. (2000), Convective inhibition, subgrid-scale triggering energy, and stratiform instability in a toy tropical wave model., *J. Atmos. Sci.*, *57*, 1515–1535.

Mapes, B. E., and R. A. Houze, Jr. (1993), Cloud clusters and superclusters over the oceanic warm pool, *Mon. Wea. Rev.*, *121*(5), 1398–1416.

Matsuno, T. (1966), Quasi-geostrophic motions in the equatorial area, *J. Meteor. Soc. Japan*, *44*(1), 25–43.

Nakazawa, T. (1986), Mean features of 30-60 day variations as inferred from 8-year OLR data, *J. Met. Soc. Japan*, *64*(5), 777–786.

Neelin, J. D., and J.-Y. Yu (1994), Modes of tropical variability under convective adjustment and the Madden–Julian oscillation. Part 1: Analytical theory, *J. Atmos. Sci.*, *51*, 1876–1894.

Neelin, J. D., and N. Zeng (2000), A quasi-equilibrium tropical circulation model—formulation, *J. Atmos. Sci.*, *57*, 1741–1766.

Ogrosky, H. R., and S. N. Stechmann (2015a), The MJO skeleton model with observation-based background state and forcing, *Q. J. Roy. Meteor. Soc.*, *141*(692), 2654–2669, doi:10.1002/qj.2552.

Ogrosky, H. R., and S. N. Stechmann (2015b), Assessing the equatorial long-wave approximation: asymptotics and observational data analysis, *J. Atmos. Sci.*, *72*, 4821–4843, doi:10.1175/JAS-D-15-0065.1.

Peters, O., J. D. Neelin, and S. W. Nesbitt (2009), Mesoscale convective systems and critical clusters, *J. Atmos. Sci.*, *66*(9), 2913–2924.

Raymond, D. J., and Ž. Fuchs (2009), Moisture modes and the Madden–Julian oscillation, *J. Climate*, *22*(11), 3031–3046.

Roundy, P., and W. Frank (2004), A climatology of waves in the equatorial region, *J. Atmos. Sci.*, *61*(17), 2105–2132.

Roundy, P. E. (2012a), Observed structure of convectively coupled waves as a function of equivalent depth: Kelvin waves and the Madden–Julian oscillation, *J. Atmos. Sci.*, *69*(7), 2097–2106, doi:10.1175/JAS-D-12-03.1.

Roundy, P. E. (2012b), The spectrum of convectively coupled Kelvin waves and the Madden–Julian oscillation in regions of low-level easterly and westerly background flow, *J. Atmos. Sci.*, *69*(7), 2107–2111, doi:10.1175/JAS-D-12-060.1.

Roundy, P. E. (2014), Regression analysis of zonally narrow components of the MJO, *J. Atmos. Sci.*, *71*(11), 4253–4275, doi:http://dx.doi.org/10.1175/JAS-D-13-0288.1.

Salby, M. L., R. R. Garcia, and H. H. Hendon (1994), Planetary-scale circulations in the presence of climatological and wave-induced heating., *J. Atmos. Sci.*, *51*, 2344–2367.

Slingo, J. M., K. R. Sperber, J. S. Boyle, J.-P. Ceron, M. Dix, B. Dugas, W. Ebisuzaki, J. Fyfe, D. Gregory, J.-F. Gueremy, J. Hack, A. Harzallah, P. Inness, A. Kitoh, W. K.-M. Lau, B. McAvaney, R. Madden, A. Matthews, T. N. Palmer, C.-K. Park, D. Randall, and N. Renno (1996), Intraseasonal oscillations in 15 atmospheric general circulation models: results from an AMIP diagnostic subproject, *Climate Dyn.*, *12*, 325–357.

Sobel, A., and E. Maloney (2013), Moisture modes and the eastward propagation of the MJO, *J. Atmos. Sci.*, *70*(1), 187–192.

Sobel, A. H., and D. Kim (2012), The MJO–Kelvin wave transition, *Geophys. Res. Lett.*, *39*(20), L20,808, doi:10.1029/2012GL053380.

Stachnik, J. P., D. E. Waliser, A. J. Majda, S. N. Stechmann, and S. Thual (2015), Evaluating MJO event initiation and decay in the skeleton model using an RMM-like index, *J. Geophys. Res. Atmos.*, *120*(22), doi:10.1002/2015JD023916.

Stechmann, S. N., and A. J. Majda (2009), Gravity waves in shear and implications for organized convection, *J. Atmos. Sci.*, *66*, 2579–2599.

Stechmann, S. N., and A. J. Majda (2015), Identifying the skeleton of the Madden–Julian oscillation in observational data, *Mon. Wea. Rev.*, *143*, 395–416, doi:10.1175/MWR-D-14-00169.1.

Stechmann, S. N., and H. R. Ogrosky (2014), The Walker circulation, diabatic heating, and outgoing longwave radiation, *Geophys. Res. Lett.*, *41*, 9097–9105, doi: 10.1002/2014GL062257.

Stechmann, S. N., A. J. Majda, and B. Khouider (2008), Nonlinear dynamics of hydrostatic internal gravity waves, *Theor. Comp. Fluid Dyn.*, *22*, 407–432.

Stechmann, S. N., A. J. Majda, and D. Skjorshammer (2013), Convectively coupled wave–environment interactions, *Theor. Comp. Fluid Dyn.*, *27*, 513–532.

Straub, K., P. Haertel, and G. Kiladis (2010), An analysis of convectively coupled Kelvin waves in 20 WCRP CMIP3 global coupled climate models, *J. Climate*, *23*(11), 3031–3056.

Straub, K. H., and G. N. Kiladis (2002), Observations of a convectively coupled Kelvin wave in the eastern Pacific ITCZ, *J. Atmos. Sci.*, *59*, 30–53.

Straub, K. H., and G. N. Kiladis (2003), The observed structure of convectively coupled Kelvin waves: comparison with simple models of coupled wave instability, *J. Atmos. Sci.*, *60*(14), 1655–1668.

Takayabu, Y. N. (1994), Large-scale cloud disturbances associated with equatorial waves. I: Spectral features of the cloud disturbances, *J. Meteor. Soc. Japan*, *72*(3), 433–449.

Takayabu, Y. N., and M. Murakami (1991), The structure of super cloud clusters observed in 1–20 June 1986 and their relationship to easterly waves, *J. Meteor. Soc. Japan*, *69*(1), 105–125.

Thual, S., and A. J. Majda (2015), A suite of skeleton models for the MJO with refined vertical structure, *Math. Clim. Weather Forecast.*, *1*, 70–95, doi:10.1515/mcwf-2015-0004.

Thual, S., A. J. Majda, and S. N. Stechmann (2014), A stochastic skeleton model for the MJO, *J. Atmos. Sci.*, *71*, 697–715.

Tulich, S. N., and G. N. Kiladis (2012), Squall lines and convectively coupled gravity waves in the tropics: Why do most cloud systems propagate westward?, *J. Atmos. Sci.*, *69*(10), 2995–3012.

Waliser, D. E., R. Murtugudde, P. Strutton, and J.-L. Li (2005), Subseasonal organization of ocean chlorophyll: Prospects for prediction based on the Madden–Julian oscillation, *Geophys. Res. Lett.*, *32*(23), doi:10.1029/2005GL024300.

Wang, B., and H. Rui (1990), Dynamics of the coupled moist Kelvin–Rossby wave on an equatorial beta-plane., *J. Atmos. Sci.*, *47*, 397–413.

Wheeler, M., and G. N. Kiladis (1999), Convectively coupled equatorial waves: analysis of clouds and temperature in the wavenumber–frequency domain, *J. Atmos. Sci.*, *56*(3), 374–399.

Wheeler, M., G. N. Kiladis, and P. J. Webster (2000), Large-scale dynamical fields associated with convectively coupled equatorial waves, *J. Atmos. Sci.*, *57*(5), 613–640.

Wood, R., and P. R. Field (2011), The distribution of cloud horizontal sizes, *J. Climate*, *24*(18), 4800–4816, doi:10.1175/2011JCLI4056.1.

Yu, J.-Y., and J. D. Neelin (1994), Modes of tropical variability under convective adjustment and the Madden–Julian oscillation. Part II: Numerical results, *J. Atmos. Sci.*, *51*(13), 1895–1914.

Zhang, C. (2005), Madden–Julian Oscillation, *Rev. Geophys.*, *43*, RG2003, doi:10.1029/2004RG000158.

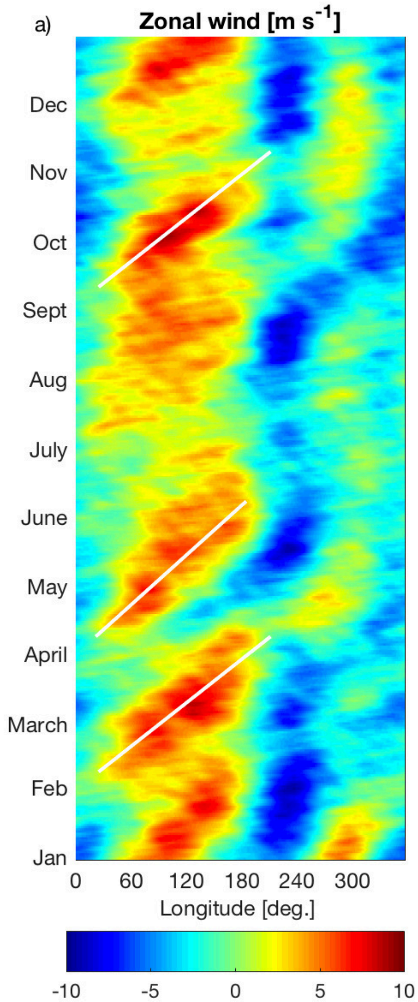


**Figure 1.** Contour plots of (a) zonal wind, $u$, and (b) precipitation, $\tau_{low}^{-1} q_{low} + \tau_{mid}^{-1} q_{mid}$, anomalies, at the equator, as functions of longitude and time, for a one-year example realization of the stochastic model dynamics of (1)–(4). Some examples of MJO events are indicated by white lines, convectively coupled equatorial Rossby wave events by white arrows, and CCKW events by black dashed lines.

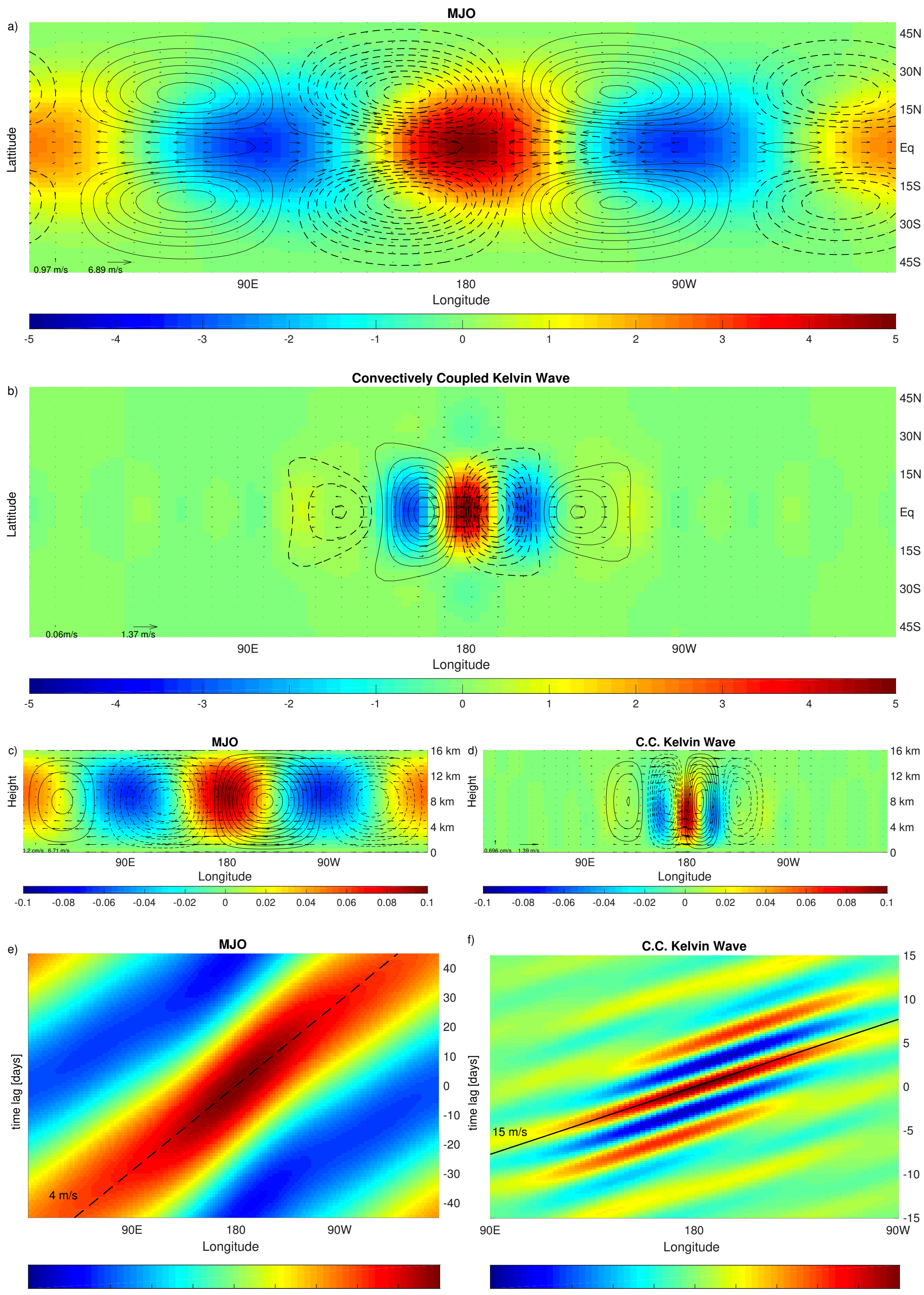


**Figure 2.** (a,b) Horizontal, (c,d) vertical, and (e,f) spatiotemporal lag-lead regressions for the MJO and CCKW. (a,b) Precipitation (mm day$^{-1}$, colors), lower-tropospheric wind vectors, and lower-tropospheric geopotential height anomalies regressed onto (scaled) precipitation anomaly. Geopotential height contour intervals are (a) 1.5 and (b) 0.25 m. Positive contours are solid black; negative contours are dashed. (c,d) Water vapor mixing ratio (g kg$^{-1}$, colors ), zonal-vertical velocity vectors, and potential temperature anomalies regressed onto (scaled) precipitation anomaly, at the equator. Potential temperature contour intervals are (c) 0.02 and (d) 0.015 K. (e,f) Precipitation anomaly (mm day$^{-1}$, colors) regressed onto itself (scaled), at the equator.

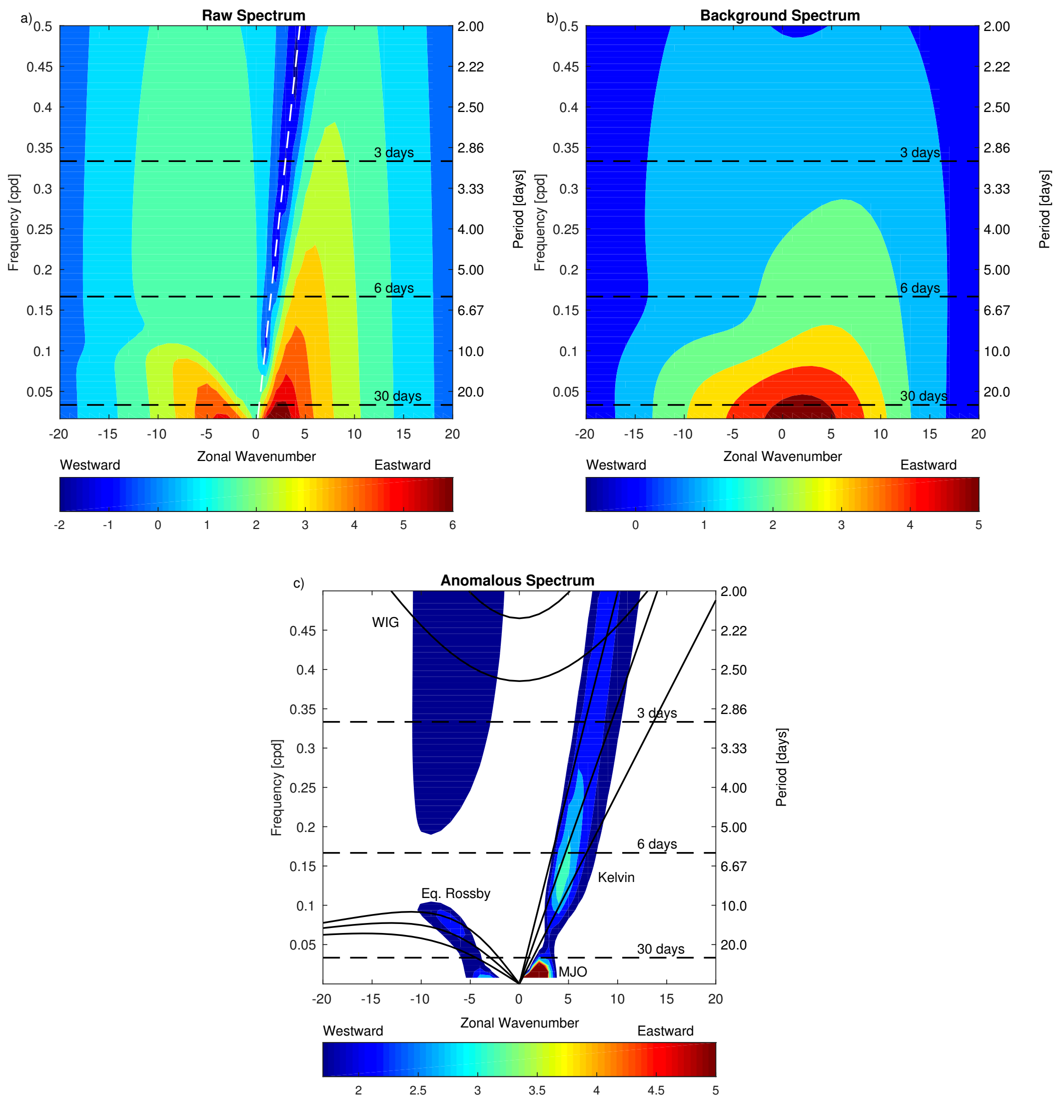


**Figure 3.** Spectral power of precipitation anomalies at the equator. (a) Raw spectrum, in logarithmic scale. White dashed line indicates a dry Kelvin wave dispersion curve with phase speed of 50 m/s. (b) Background spectrum, obtained by smoothing the raw spectrum, using methods of *Wheeler and Kiladis* [1999]. (c) Anomalous spectrum, obtained by scaling the raw spectrum by the background spectrum. Black curves indicate the dispersion curves of the dry equatorial shallow water equations for equivalent depths of 12, 25, and 50 m.

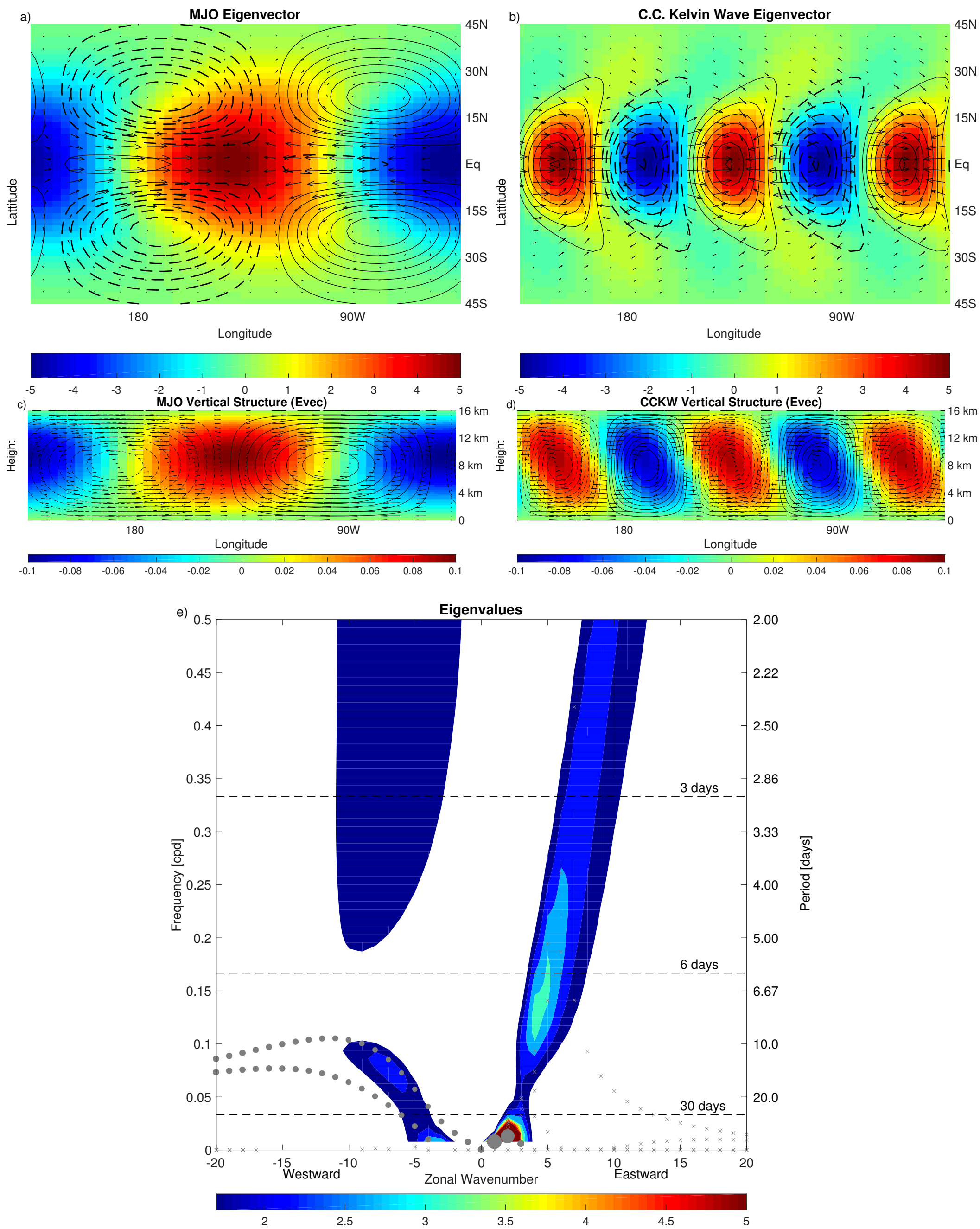


**Figure 4.** Eigenvectors and eigenvalues of the deterministic part of the model in (1)–(4). (a,c) MJO eigenmode, zonal wavenumber $k = 2$. (b,d) CCKW eigenmode, zonal wavenumber $k = 5$. (A different type of CCKW eigenmode with $k = 5$ is shown in the SI in Fig. S1.) Color shading and contours drawn as in Fig. 2, except contour intervals are (a) 1.5 m, (b) 0.56 m, (c) 0.02 K, and (d) 0.03 K. (e) Eigenvalues of modes that are symmetric with respect to the equator, superposed on color contours of anomalous power spectrum from Fig. 3c. Circle radius is proportional to eigenmode damping time scale, with crosses displayed instead of circles if the damping time scale is shorter than 2.4 days. For the MJO eigenmodes at $k = 1, 2$, and 3, the damping time scales are 48, 44, and 10 days, respectively.